



# Isotope Exchange Reaction of OH<sup>-</sup> Anion with HD at Temperatures from 15 K up to 300 K: Ion Trap Study

Radek Plašil , Liliia Uvarova , Serhiy Rednyk , Štěpán Roučka , Erik Vanko , Petr Dohnal , and Juraj Glosík   
Charles University, Faculty of Mathematics and Physics, Department of Surface and Plasma Science, V Holešovičkách 2, 180 00 Prague, Czech Republic; [radek.plasil@mff.cuni.cz](mailto:radek.plasil@mff.cuni.cz)

Received 2023 January 30; revised 2023 March 30; accepted 2023 March 30; published 2023 May 17

## Abstract

This paper presents the results of an experimental study of the reaction of OH<sup>-</sup> anions with HD molecules leading to the formation of OD<sup>-</sup> anions. The study's main goal was to obtain the temperature dependence of the reaction rate coefficient and determine the reaction's enthalpy. This study was carried out at astrophysically relevant temperatures from 15 to 300 K. The reaction was studied using a temperature-variable cryogenic linear 22-pole radio-frequency ion trap. The rotational temperature of the OH<sup>-</sup> anions in the ion trap was characterized by near-threshold photodetachment spectroscopy. At 15 K, the measured reaction rate coefficient is  $5 \times 10^{-10} \text{ cm}^3 \text{ s}^{-1}$ . With increasing temperature, the reaction rate coefficient decreases monotonically to  $5 \times 10^{-11} \text{ cm}^3 \text{ s}^{-1}$  at 300 K. Comparing with the previously determined rate coefficient of the reverse reaction of OD<sup>-</sup> anions with H<sub>2</sub>, we obtained the temperature dependence of the equilibrium constant. The enthalpy and entropy of the title reaction were determined in the studied temperature range as  $\Delta H = (-23.9 \pm 0.7 \pm 2.6^{\text{sys}}) \text{ meV}$  and  $\Delta S = (-8.5 \pm 1.2 \pm 1.4^{\text{sys}}) \text{ J mol}^{-1} \text{ K}^{-1}$ , respectively.

*Unified Astronomy Thesaurus concepts:* [Astrochemistry \(75\)](#); [Interstellar molecules \(849\)](#); [Isotopic abundances \(867\)](#); [Laboratory astrophysics \(2004\)](#); [Reaction rates \(2081\)](#)

## 1. Introduction

Herbst (1981) suggested that a substantial fraction of molecular material in interstellar space may be in the form of anions. Recent studies have proved that negative ions play an important role in many gaseous astrophysical environments ranging from Earth's ionosphere, and planetary atmospheres, through stellar photospheres to dark interstellar clouds (Desai et al. 2021). Anions are also crucial for many technological applications and plasma technologies.

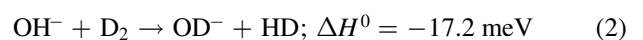
Until 2006, there was agreement about the role of H<sup>-</sup> in stellar photospheres. However, there was no evidence of the presence of anions in interstellar media. Then McCarthy et al. (2006) measured spectra of C<sub>6</sub>H<sup>-</sup> in a laboratory and identified them in the dense molecular cloud TMC-1. Many other observations of anions followed (Millar et al. 2017; Remijan et al. 2023). Anions were observed in many interstellar environments, from quiescent molecular clouds to star-forming regions. The rotational spectrum of OH<sup>-</sup> is well known (Jusko et al. 2014) with the fundamental  $J=1 \leftarrow 0$  (1.123 THz) transition with sufficiently high values of Einstein coefficients for observation (Endres et al. 2016). Moreover, the spectrum of OH<sup>-</sup> is simple because it is a closed-shell molecule.

Despite the relatively high electron affinity of OH, 1.83 eV (Schulz et al. 1982), the hydroxyl anion OH<sup>-</sup> has not yet been observed in interstellar space, even though the hydroxyl radical OH was observed as the first molecule using radio astronomy (Weinreb et al. 1963) and the hydroxyl cation OH<sup>+</sup> has also been observed (Wyrowski et al. 2010). Up-to-date models predict similar number densities of OH<sup>-</sup> and OH<sup>+</sup> in dark interstellar clouds (McElroy et al. 2013).

The peak in the mass spectrum corresponding to the hydroxyl anion OH<sup>-</sup> was detected in the coma of comet Halley (Chaizy et al. 1991). The present chemical models cannot explain such a high number density in the photon-dominated region near the Sun, where photodetachment plays an important role. Cordiner & Charnley (2014) reported a difference of two orders of magnitude between the values obtained by the model and the observation of Chaizy et al. (1991). Other models also predict the presence of OH<sup>-</sup> in Titan's atmosphere (Mukundan & Bhardwaj 2018). Also, its isotopologue OD<sup>-</sup> can be considered a suitable candidate for interstellar observation because its rotational transitions are in an accessible range (Lee et al. 2016).

The importance of the OH<sup>-</sup> anion is evident from a large number of current laboratory and theoretical studies of its formation and destruction (Hlavenka et al. 2009; Hauser et al. 2015a; Jusko et al. 2015; Plašil et al. 2017) and from many other studies of its properties (Cazzoli & Puzzarini 2006; Matsushima et al. 2006; Jusko et al. 2014; Hauser et al. 2015b; Lee et al. 2016). OH<sup>-</sup> is also often used to characterize the kinetic temperature, internal excitation, and other parameters of ions in ion traps (Otto et al. 2013; Endres et al. 2017) and ion storage rings (Meyer et al. 2017; Schmidt et al. 2017).

The destruction and the formation of the OH<sup>-</sup> anions in an astrophysical low-temperature environment can be influenced by the reactions of OH<sup>-</sup> and OD<sup>-</sup> anions with H<sub>2</sub>, HD, and D<sub>2</sub>:



The enthalpies of the reactions at 0 K,  $\Delta H^0$ , were calculated in the Born–Oppenheimer approximation from the electron affinities of OH<sup>-</sup> and OD<sup>-</sup> (Schulz et al. 1982; Smith et al.

1997) and zero-point vibrational energies of  $\text{H}_2$ , HD,  $\text{D}_2$ , OH, and OD (Huber & Herzberg 1979; Rosenbaum et al. 1986; Irikura 2007). The experimental study of reaction (1) is the subject of the present study. Reactions (2) and (3) were previously studied mostly in swarm experiments at 300 K and at pressures of hundreds of pascals (Mautner et al. 1980; Grabowski et al. 1983; Viggiano & Morris 1994). Some of these reactions were studied in our laboratory at temperatures below 300 K using a temperature-variable radio-frequency ion trap. Recently we studied the isotope exchange reactions  $\text{OH}^- + \text{D}_2$  and  $\text{OD}^- + \text{H}_2$  (Mulin et al. 2015; Roučka et al. 2018). Note that reaction (1) is the reverse of reaction (3). The temperature dependences of the rate coefficients of the above reactions are very sensitive to the corresponding reaction enthalpies. This is especially true at low temperatures, which are typical for conditions in interstellar media.

The present study is focused on the exothermic H/D exchange reaction of  $\text{OH}^-$  with HD (1). In the evaluation of  $\Delta H^0$  of this reaction, we will use the results from our recent experimental study of the reaction of  $\text{OD}^-$  with  $\text{H}_2$  (3), where we characterized the effect of rotational excitation of  $\text{H}_2$  on the temperature dependence of the reaction rate coefficient using normal and para-enriched  $\text{H}_2$  reactant gas (Roučka et al. 2018).

## 2. Experiment—Cryogenic Ion Trap

To study the reaction of  $\text{OH}^-$  with HD, we have used a temperature-variable cryogenic linear 22-pole radio-frequency (RF) ion trap (22PT). The principle of ion trapping, the details of the apparatus used, and operating procedures have been described previously (Gerlich 1992, 1995; Gerlich et al. 2011; Plašil et al. 2011; Zymak et al. 2013). We will give only a short description and emphasize some specific aspects of the present study here. The configuration of the experiment is shown schematically in Figure 1. The 22-pole ion trap is placed in a copper box attached to the cold head of the closed-cycle helium refrigerator and can be cooled down to 10 K. The reactant gas is leaked into the cooled copper box that surrounds the 22-pole trap. The nominal trap temperature,  $T_{22\text{PT}}$ , is measured using a silicon diode attached to the copper box. The trap temperature can be varied between 10 and 300 K.

In the present experiments, the primary  $\text{OH}^-$  anions are produced by electron bombardment of the source gas in the storage ion source (SIS). In the ion source, a mixture of  $\text{N}_2\text{O}$  and  $\text{H}_2$  is used as the source gas. For formation details, see Smit & Field (1977). Anions formed in the SIS are periodically extracted and mass-selected by a quadrupole mass filter. Mass-selected anions are injected via a quadrupole bender into the 22PT ion trap (Gerlich et al. 2013; Zymak et al. 2013; Plašil et al. 2022).

In the standard measuring procedure, primary reactant ions (in the present studies, the  $\text{OH}^-$  anions) are periodically injected into the trap. At fixed conditions in the ion source, the trap is filled with a well-defined number of primary ions. After a certain trapping (reaction) time, the reactant and product ions are extracted from the ion trap. After passing through a quadrupole mass spectrometer, they are counted using a microchannel plate detector; see Figure 1. By repetition of this procedure for different trapping times, one can obtain the time evolution of the relative number of anions of a particular mass in the ion trap. In the following text, the number of ions detected after time  $t$  is denoted as  $N_X(t)$ , where index  $X$  refers to a particular type of ion. In particular, the relative numbers of

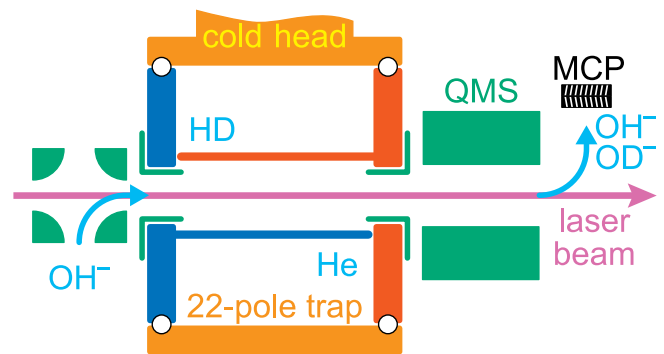


**Figure 1.** Scheme of the linear 22-pole ion trap. In the radial direction, the ions are confined by a radio-frequency field created by two sets of 11 poles mounted precisely on opposite sides. The entrance and exit electrodes are used to open and close the trap by means of electrostatic barriers. The ions are analyzed using a quadrupole mass spectrometer (QMS) and counted using a microchannel plate (MCP).

$\text{OH}^-$  and  $\text{OD}^-$  anions, denoted by  $N_{\text{OH}^-}$  and  $N_{\text{OD}^-}$ , respectively, were measured for several HD densities as a function of time after injection of  $\text{OH}^-$  anions into the trap.

We continuously introduce the reactant into the trap volume, and the total pressure is measured by a spinning rotor gauge. We estimate the systematic uncertainty of reactant number density as 20%. The isotopic enrichment of HD gas is 97%, according to the manufacturer Cambridge Isotope Laboratories, Inc., Tewksbury, MA, USA.

The mass discrimination connected with the extraction from the ion trap and detection of ions of different masses was considered in the data analysis. It was found to be negligible within the accuracy of the present data; the relative difference in detection efficiencies is less than 5%. For a detailed description, see, e.g., Roučka et al. (2018).

### 2.1. Reactant Temperature

The actual translational and internal temperature of reactants can deviate from the nominal temperature of the trap, as discussed below. The temperature of the trap rods can be higher due to their resistive RF heating, and consequently the temperature of the reactant gas may be elevated. The RF electric field can also heat the ions in the trap. This heating depends on the particular construction of the trap, the RF frequency, and RF amplitude. Accordingly, the trapped ions can have higher kinetic energy than the energy corresponding to the temperature of the trap.

We will assume that the kinetic energy distribution of the trapped ions is close to a Maxwell–Boltzmann distribution and can be characterized by the kinetic temperature  $T_{\text{kin}}$ . The kinetic temperature of stored ions under particular experimental conditions can be characterized by measuring the Doppler broadening of suitable absorption lines of trapped ions (Glosik et al. 2006; Jusko et al. 2014; Kovalenko et al. 2021; Nötzold et al. 2022).

Several recent experiments established that the collision energies in collisions between ions and reactant molecules can be characterized by a collisional temperature, here denoted as  $T$ . This collisional temperature does not exceed  $T_{22\text{PT}}$  by more than 10 K. For the presentation of our data we define the collisional temperature as  $T = T_{22\text{PT}} + (5 \pm 5)$  K. For further details and discussion see Plašil et al. (2012), Zymak et al. (2013), Hauser et al. (2015b), Endres et al. (2017), and Roučka et al. (2018).

**Table 1**

The List of Transitions and Corresponding Threshold Energies Used in the Present Study

Transition	Threshold Energy $\varepsilon$ (cm <sup>-1</sup> )	Transition	Threshold Energy $\varepsilon$ (cm <sup>-1</sup> )
O <sub>3</sub> (4)	14,450.8	P <sub>1</sub> (3)	14,703.6
O <sub>3</sub> (3)	14,516.4	Q <sub>3</sub> (2)	14,712.5
P <sub>3</sub> (4)	14,569.1	Q <sub>3</sub> (3)	14,718.8
P <sub>3</sub> (3)	14,600.2	Q <sub>3</sub> (4)	14,723.0
P <sub>3</sub> (2) <sup>a</sup>	14,628.6	R <sub>3</sub> (0) <sup>a</sup>	14,740.9
P <sub>1</sub> (4)	14,655.7	R <sub>3</sub> (1)	14,787.2
Q <sub>3</sub> (1) <sup>a</sup>	14,703.5	Q <sub>1</sub> (4)	14,796.1

**Note.**<sup>a</sup> Only these transitions were considered in the study by Otto et al. (2013).

### 3. Thermalization of OH<sup>-</sup> Anions

The actual internal excitation of OH<sup>-</sup> anions depends on the effectiveness of quenching in collisions with He atoms. Since the studied reaction (1) is nearly thermoneutral and as such can be very sensitive to the internal excitation of the reactants, we decided to characterize the internal (rotational) excitation of the trapped ions by near-threshold photodetachment spectroscopy (Otto et al. 2013; Endres et al. 2017, 2021).

In the photodetachment experiments, we covered the temperature range of  $T_{22PT}$  from 50 to 200 K. In contrast with the study of Otto et al. (2013) performed for temperatures below 50 K, we have to consider also higher-lying rotational states and more photodetachment thresholds and corresponding transitions; for details see Table 1. Two laser diodes (QL68j6SA by Quantum Semiconductor International Co., Ltd. covering the range 14,600–14,670 cm<sup>-1</sup> and HL6756MG by Ushio Inc. in the range 14,680–14,820 cm<sup>-1</sup>) were used as light sources. The wavelength was measured absolutely by an Exfo WA-1650 wave meter.

Following Otto et al. (2013), the photodetachment cross section, which is proportional to the measured loss rate of OH<sup>-</sup> ions in the trap, can be described by the formula for the photon energies above the thresholds; otherwise, the term in the sum is zero:

$$\sigma(h\nu) = A \sum_{Jn} P(J) I_{Jn} (h\nu - \varepsilon_{Jn})^p, \quad (5)$$

where  $A$  is a proportionality constant,  $h\nu$  is the photon energy,  $P(J)$  is the population of the rotational level of the OH<sup>-</sup> anion with rotational quantum number  $J$ ,  $I_{Jn}$  and  $\varepsilon_{Jn}$  are the corresponding Hönl–London factors and threshold energies (Goldfarb et al. 2005), and  $p$  is 0.28 following Engelking (1982). The summation goes over all rotational levels ( $J$ ) and corresponding transitions ( $n$ )—more than one transition can originate in a given rotational energy level.

To evaluate the rotational temperature, we fitted the measured frequency dependence of the photodetachment rate by two model functions based on formula (5). In the first model, we assumed that the rotational states with corresponding energy  $E_J$  are populated in accordance with thermal equilibrium at temperature  $T$ :

$$P(J, T) = \frac{2J+1}{Z} \exp\left(\frac{-E_J}{k_B T}\right), \quad (6)$$

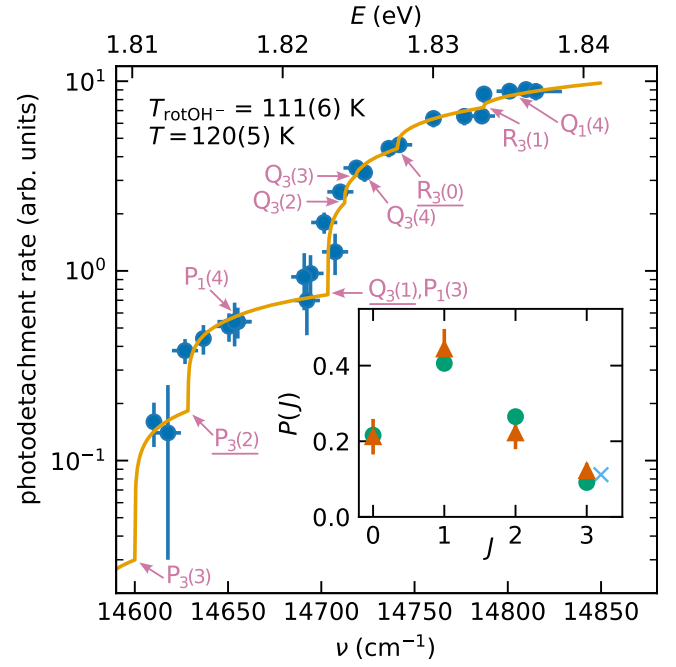


**Figure 2.** Photodetachment rate at collisional temperature  $T = 120$  K and  $[\text{He}] = 5.5 \times 10^{13} \text{ cm}^{-3}$ . The obtained rotational temperature is  $T_{\text{rotOH}^-} = 111(6)$  K. The full line denotes the fit of the data by formula (5) under the assumption of the thermal population of states with temperature as a free parameter. Only the underlined transition labels were considered in the study by Otto et al. (2013). Inset: the relative populations of the lowest rotational states of the OH<sup>-</sup> anion (triangles) determined from the fit of the obtained data by Equation (6) with the populations of rotational states up to  $J = 3$  as free parameters. The calculated thermal populations at 115 K are plotted as circles. Due to the position of the corresponding photodetachment thresholds, the value obtained for  $J = 3$  consists of indistinguishable contributions from states with  $J = 3, 4$ , and 5. A cross denotes the sum of the calculated relative thermal populations of these states.

where  $Z$  is the partition function. The ratio  $A/Z$  and the rotational temperature  $T$  are the only parameters of this model.

In the second model, the fit parameters are the constant  $A$  and the populations of the OH<sup>-</sup>  $P(J)$  rotational states. The first model fitted to the data obtained at  $T = 120$  K (trap temperature of  $T_{22PT} = 115$  K) is plotted in Figure 2. The rotational populations obtained from the fit of the second model are displayed in the inset of Figure 2 and compared to thermal data. The dependence of the measured rotational temperature of OH<sup>-</sup> on the collisional temperature is shown in Figure 3.

### 4. Results

Typical measured time evolutions of the numbers of detected primary OH<sup>-</sup> and product OD<sup>-</sup> anions are shown in Figure 4. The actual measurements were performed at the following temperatures and HD number densities:  $T = 135$  K,  $[\text{HD}] = 5.0 \times 10^{10} \text{ cm}^{-3}$  (upper panel) and  $T = 36$  K,  $[\text{HD}] = 1.0 \times 10^{11} \text{ cm}^{-3}$  (lower panel). For a longer trapping time, we can see leveling of the number of OH<sup>-</sup> anions due to the back-conversion of OD<sup>-</sup> anions in reactions with HD and with residual H<sub>2</sub> from the ion source in reactions (3) and (4). The data were analyzed by least-squares fitting the measured numbers of ions with a kinetic model characterized by time derivatives of the ion counts:

$$\dot{N}_{\text{OH}^-} = -(r_1 + r_{\text{loss}})N_{\text{OH}^-} + r_b N_{\text{OD}^-} \quad (7)$$

$$\dot{N}_{\text{OD}^-} = r_1 N_{\text{OH}^-} - (r_b + r_{\text{loss}})N_{\text{OD}^-}. \quad (8)$$

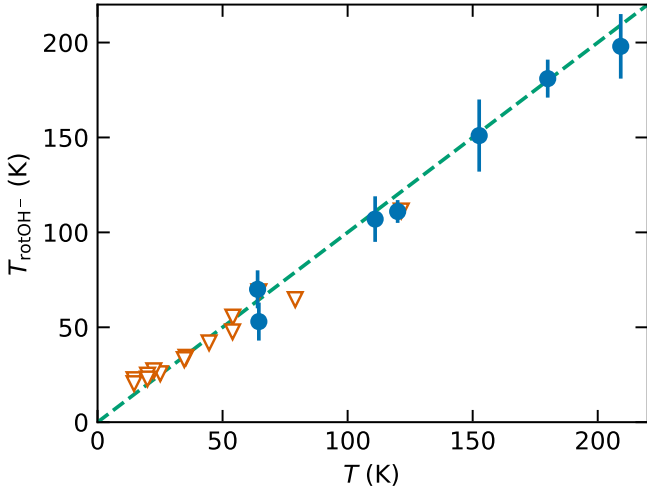


**Figure 3.** Dependence of the measured rotational temperature  $T_{\text{rotOH}^-}$  of the  $\text{OH}^-$  ions on the collisional temperature  $T = T_{22\text{PT}} + 5 \text{ K}$ . The values of  $T_{\text{rotOH}^-}$  were obtained by fitting the measured photodetachment rates using formula (5) under the assumption of the thermal population of states (solid circles). The displayed errors are statistical errors of the fit. The number densities of helium buffer gas were in the range  $(4\text{--}8) \times 10^{13} \text{ cm}^{-3}$ . Data obtained by the same technique using a similar experimental setup by Endres et al. (2017) are plotted as a function of  $T = T_{22\text{PT}}^{\text{Endres}} + 5 \text{ K}$  for comparison with our data (open triangles). The dashed line indicates identity  $T_{\text{rot}} = T$ .

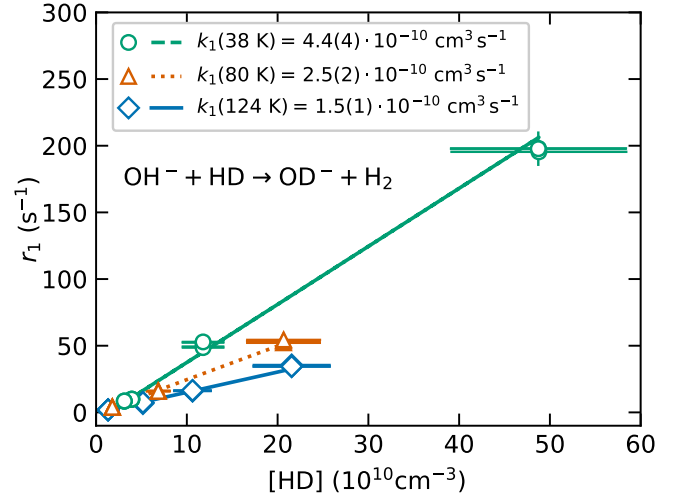


**Figure 5.** The dependences of the reaction rates  $r_1$  on  $[\text{HD}]$  measured at collisional temperatures  $T = 38 \text{ K}$  (circles,  $[\text{He}] = 9.7 \times 10^{13} \text{ cm}^{-3}$ ),  $T = 80 \text{ K}$  (triangles,  $[\text{He}] = 6.8 \times 10^{13} \text{ cm}^{-3}$ ), and  $T = 124 \text{ K}$  (diamonds,  $[\text{He}] = 5.4 \times 10^{13} \text{ cm}^{-3}$ ). The primary  $\text{OH}^-$  anions were produced in the SIS and injected into the ion trap. The slope of the plotted dependences gives the values of the corresponding binary reaction rate coefficients  $k_1$  (see the text). The reaction rate coefficients obtained at different temperatures in these particular experiments are indicated in the figure.

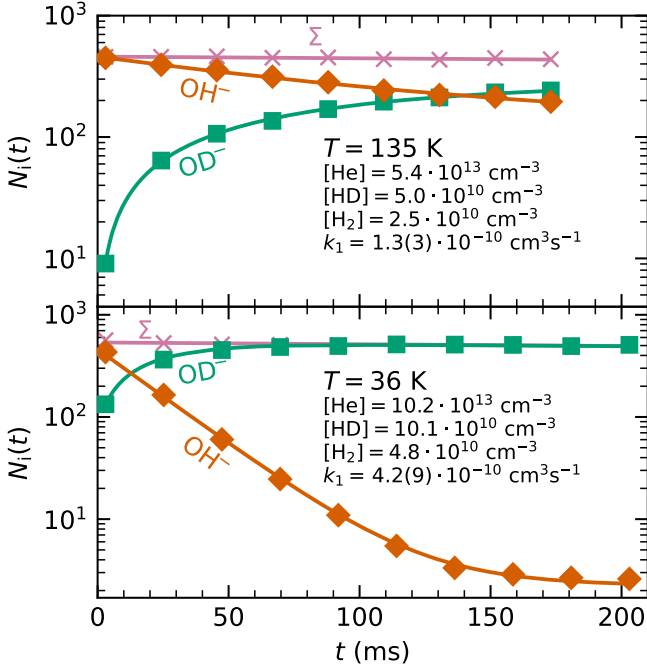


**Figure 4.** Time evolutions of the numbers of detected primary  $\text{OH}^-$  and produced  $\text{OD}^-$  anions (diamonds and squares, respectively) as a function of the trapping time. The data were measured at the indicated temperatures (upper panel:  $T = 135 \text{ K}$ , lower panel:  $T = 36 \text{ K}$ ). The time evolutions of the total numbers of detected  $\text{OH}^-$  and  $\text{OD}^-$  anions ( $\Sigma$ , crosses) are also indicated. The experimental conditions and the evaluated rate coefficients of reaction (1) including their overall uncertainties are indicated in the figure.

The initial numbers  $N_{\text{OH}^-}(t = 0)$ ,  $N_{\text{OD}^-}(t = 0)$  and rates  $r_1$ ,  $r_b$ ,  $r_{\text{loss}}$  were free parameters. The rate  $r_1$  of reaction (1) is related to the rate coefficient as  $r_1 = k_1 \times [\text{HD}]$ . The rate  $r_b$  accounts for the back-conversion of  $\text{OD}^-$  to  $\text{OH}^-$  in reactions (3) and (4). The loss rate  $r_{\text{loss}}$ , which accounts for the loss of ions due

to reactions with impurities and leakage from the trap, is assumed to be equal for both  $\text{OH}^-$  and  $\text{OD}^-$ . It is negligible at temperatures below 200 K.

To confirm the binary character of the reaction of  $\text{OH}^-$  with HD taking place in the ion trap under the experimental conditions used, the dependence of the reaction rate  $r_1$  of reaction (1) on the reactant number density  $[\text{HD}]$  was measured at several temperatures under otherwise identical conditions. The examples of the dependences of  $r_1$  on  $[\text{HD}]$  obtained from the data measured at  $T = 38, 80,$  and  $124 \text{ K}$  are shown in Figure 5. The linearity of the obtained dependences confirms that the time evolutions of the number of  $\text{OH}^-$  ions in the ion trap are controlled by the binary reaction of  $\text{OH}^-$  anions with HD. The values of the corresponding binary reaction rate coefficient  $k_1$  are given by the slope of the plotted dependences. The dependence of the reaction rate  $r_1$  on  $[\text{He}]$  was also monitored in the experiments, but we did not find any significant variation by increasing  $[\text{He}]$  from  $10^{12} \text{ cm}^{-3}$  to  $2 \times 10^{14} \text{ cm}^{-3}$ .

By measuring the time evolutions of the numbers of particular anions in the ion trap at temperatures from 15 K up to 300 K, the temperature dependence of the rate coefficient  $k_1$  of reaction (1) was obtained. The obtained raw data and final temperature dependence of the rate coefficient  $k_1$  of the reaction of  $\text{OH}^-$  anions with HD are shown in Figure 6.

To facilitate the use of our data in astrochemical models, we fitted the temperature dependence of  $k_1$  with the modified Arrhenius formula  $k_1 = \alpha(T/300 \text{ K})^\beta \exp(-\gamma/T)$ . The fit is in good agreement with the data, as shown in Figure 6, and the fitted parameters are  $\alpha = 5.1(3) \times 10^{-11} \text{ cm}^3 \text{ s}^{-1}$ ,  $\beta = -1.29(9)$ , and  $\gamma = 23(5) \text{ K}$ .

## 5. Discussion

The combination of the reaction rate coefficient  $k_1$  obtained in the present study with the rate coefficient of the reverse reaction (3) of  $\text{OD}^-$  with  $\text{H}_2$  allows us to evaluate the reactions'



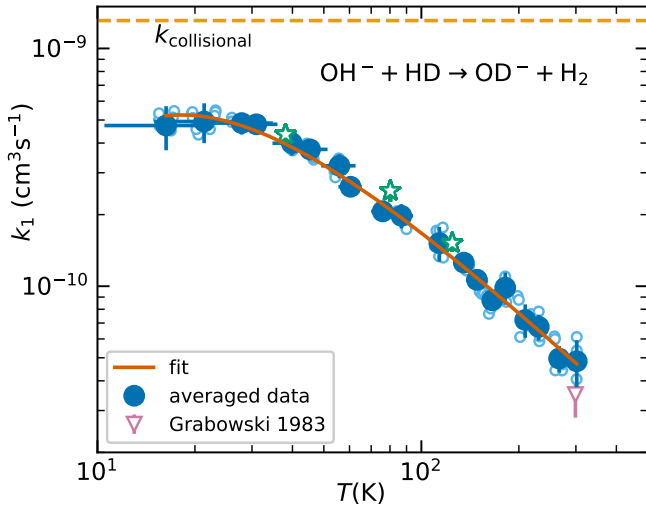


**Figure 6.** Temperature dependence of the rate coefficient  $k_1$  measured for the H/D exchange reaction (1) of  $\text{OH}^-$  with HD. The raw and averaged data measured in the present experiments with the injection of  $\text{OH}^-$  anions into the ion trap are indicated by the open and solid circles, respectively. The reaction rate coefficients obtained from the slopes of the  $[\text{HD}]$  dependences (Figure 5) are indicated by the stars. The open triangle indicates the value of the reaction rate coefficient  $k_1(299 \text{ K}) = 3.5 \times 10^{-11} \text{ cm}^3 \text{ s}^{-1}$  measured in the SIFT experiment by Grabowski et al. (1983). The corresponding collisional rate coefficient of  $1.31 \times 10^{-9} \text{ cm}^3 \text{ s}^{-1}$  (dashed line) was calculated using Langevin theory and the polarizability of HD by Kolos & Wolniewicz (1967), neglecting its permanent dipole moment (Su & Chesnavich 1982).

equilibrium constant and endothermicity. Measured temperature dependences of the rate coefficients  $k_1$  and  $k_3$  in the form of the Arrhenius plot are shown in Figure 7. The thermal values of  $k_3$  are calculated from the data measured with para-enriched  $\text{H}_2$  and normal  $\text{H}_2$  using the 22-pole ion trap (Mulin et al. 2015; Roučka et al. 2018). Also shown are values of  $k_1$  and  $k_3$  obtained at 299 K in a SIFT study of Grabowski et al. (1983) ( $k_1(299 \text{ K}) = 3.5 \times 10^{-11} \text{ cm}^3 \text{ s}^{-1}$ ,  $k_3(299 \text{ K}) = 3.8 \times 10^{-11} \text{ cm}^3 \text{ s}^{-1}$ ).

Since reactions (1) and (3) are mutually inverse, we can accurately analyze the reaction endothermicity by calculating their equilibrium constant,  $K_{\text{eq}}(T)$ . In further analysis, we will treat reactions (3) and (1) as the forward and reverse reactions. The equilibrium constant can be expressed by the formula

$$K_{\text{eq}}(T) = k_3/k_1. \quad (9)$$

Furthermore, the equilibrium constant is related to the standard reaction Gibbs energy,  $\Delta_r G^\ominus$ , as  $RT \ln(K_{\text{eq}}(T)) = -\Delta_r G^\ominus$  (see, e.g., Atkins et al. 2018, chapter 6), and considering the definition of the Gibbs energy, we obtain the following relationship between the equilibrium constant and the standard reaction enthalpy and entropy:

$$\ln(K_{\text{eq}}(T)) = -\Delta_r H^\ominus(T)/RT + \Delta_r S^\ominus(T)/R. \quad (10)$$

In the dilute gas, where the enthalpy of mixing is negligible, the enthalpy and entropy are pressure-independent, and we will denote them simply as  $\Delta H(T)$  and  $\Delta S(T)$ . The conventional method for interpreting the measured equilibrium constant assumes that the reaction enthalpy and entropy are constant with respect to temperature. This allows the measured  $\ln(K_{\text{eq}}(T))$  to be fitted as a linear function of  $1/T$  with the slope and intercept of the fitted line given by  $-\Delta_r H(T)/R$  and  $\Delta_r S(T)/R$ , respectively. The Van't Hoff plot of the measured equilibrium constant shown in Figure 8 confirms the validity

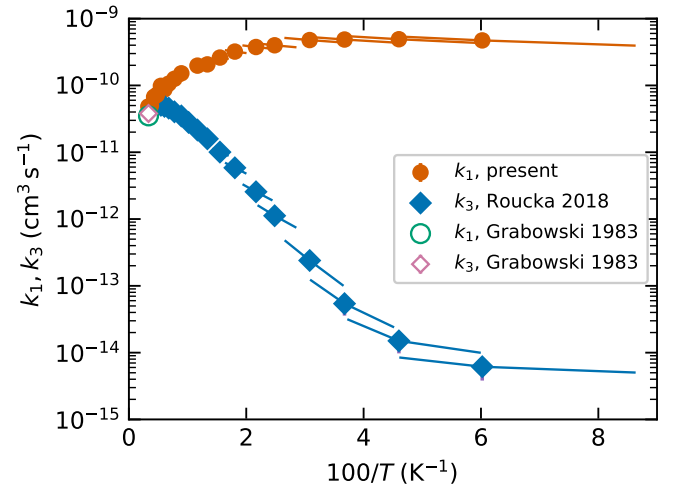


**Figure 7.** Arrhenius plots of the rate coefficients of reaction (1) ( $k_1$ , solid circles) obtained in the present study and those of reaction (3) ( $k_3$ , solid diamonds). The thermal values of  $k_3$  are calculated from the data measured with para-enriched  $\text{H}_2$  and normal  $\text{H}_2$  (Roučka et al. 2018). The thermal values of  $k_1$  and  $k_3$  obtained at 299 K in the SIFT experiment of Grabowski et al. (1983) are indicated by the open circle and open diamond, respectively.

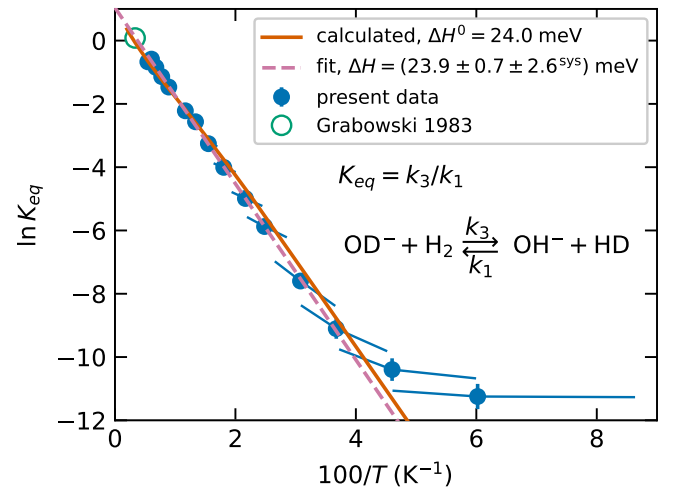


**Figure 8.** Van't Hoff plot of the equilibrium constant  $K_{\text{eq}} = k_3/k_1$  of the reactions (3) and (1). The solid points indicate the data calculated from the values of  $k_1$  measured in the present experiments and from  $k_3$  adapted from Roučka et al. (2018). The open circle indicates the value measured by Grabowski et al. (1983). The dashed line was obtained by the linear fit and the solid line indicates the calculated function  $K_{\text{eq}}(T)$  with  $\Delta H^0$  given by the Born–Oppenheimer approximation.

of this assumption within the accuracy of our data. The parameters obtained from the linear fit are  $\Delta H = (23.9 \pm 0.7 \pm 2.6^{\text{sys}}) \text{ meV}$  and  $\Delta S = (8.5 \pm 1.2 \pm 1.4^{\text{sys}}) \text{ J mol}^{-1} \text{ K}^{-1}$ .

The first part of the uncertainty contains the statistical error and the error due to pressure uncertainty. In contrast, the second term includes systematic error due to temperature uncertainty. The fitted value of  $\Delta H$  perfectly agrees with the 0 K enthalpy of reaction (3) estimated using the Born–Oppenheimer approximation as  $\Delta H^0 = 24.0 \text{ meV}$  (Mulin et al. 2015). Note that this agreement is not obvious, because the fitted value of  $\Delta H$  and the calculated value of  $\Delta H^0$  rely on the assumptions of the constant value of  $\Delta H$  and  $\Delta S$  and the existence of an isotope-independent Born–Oppenheimer potential energy surface, respectively.

The first assumption can be corroborated if we calculate the equilibrium constant from the partition functions of the reactants and products as

$$K_{\text{eq}} = \left( \frac{\mu_{\text{OH}^-, \text{HD}}}{\mu_{\text{OD}^-, \text{H}_2}} \right)^{3/2} \frac{q_{\text{OH}^-} q_{\text{HD}}}{q_{\text{OD}^-} q_{\text{H}_2}} \exp\left(-\frac{\Delta H^0}{k_B T}\right), \quad (11)$$


where  $q_X$  denotes the internal partition sum of species  $X$ , and  $\mu_{X,Y}$  is the reduced mass of species  $X$  and  $Y$  (Light et al. 1969, page 313). At temperatures below 300 K, it is sufficient to consider only the rotational and hyperfine structure in calculating the partition functions, because excited vibrational or electronic states are not significantly populated. The rotational constants of all reactants and products are known with good accuracy (Huber & Herzberg 1979; Rehfuss et al. 1986; Matsushima et al. 2006; Jusko et al. 2014). Thus the only uncertain parameter is the energy difference between ground-state products and reactants given by the 0 K reaction enthalpy,  $\Delta H^0$ . We used the  $\Delta H^0$  value from the Born–Oppenheimer approximation to calculate the equilibrium constant shown in Figure 8. A comparison of the calculated equilibrium constant with the linear fit shows that there is indeed a slight nonlinearity. However, the calculated equilibrium constant is (within the estimated errors) in perfect agreement with the measured data. This confirms that  $\Delta H^0$  is accurately predicted by the Born–Oppenheimer approximation. We estimate that the error due to isotope electronic shifts does not exceed 2.4 meV (the overall uncertainty of the fitted  $\Delta H$ ). This value is in accord with our previous upper estimates of the isotope electronic shifts of 2.5 meV (Mulin et al. 2015).

## 6. Conclusions

Using the temperature-variable cryogenic linear 22-pole radio-frequency ion trap, we measured the temperature dependence of the rate coefficient  $k_1$  of the isotope exchange reaction of  $\text{OH}^-$  with HD at temperatures from 15 to 300 K; see Figure 6. The rotational temperature of the  $\text{OH}^-$  anions in the ion trap was characterized by measuring the near-threshold photodetachment spectra. We used the measured temperature dependence of  $k_1$  and the reverse reaction rate coefficient,  $k_3(T)$  (Mulin et al. 2015; Roučka et al. 2018), to determine the temperature dependence of the corresponding equilibrium constant  $K_{\text{eq}}(T) = k_3/k_1$ . The equilibrium constant is well approximated by a linear function in the Van't Hoff plot with the enthalpy and entropy of reaction (1) given by  $\Delta H = (-23.9 \pm 0.7 \pm 2.6^{\text{sys}}) \text{ meV}$  and  $\Delta S = (-8.5 \pm 1.2 \pm 1.4^{\text{sys}}) \text{ J mol}^{-1} \text{ K}^{-1}$ , respectively. The experimentally determined reaction enthalpy agrees with the 0 K reaction enthalpy calculated within the Born–Oppenheimer approximation as  $\Delta H^0 = 24.0 \text{ meV}$ , indicating that the isotopic electronic shifts between the  $\text{OD}^-$  and  $\text{OH}^-$  potential energy surfaces are less than 2.4 meV, in accord with our previous estimates.

We thank the Technische Universität Chemnitz and the Deutsche Forschungsgemeinschaft for lending the 22-pole trap to the Charles University. This work was funded by the Czech Science Foundation projects No. 20-22000S. Students' work was supported by the Charles University Grant Agency project Nos. 376721 and 332422.

## ORCID iDs

Radek Plašil  <https://orcid.org/0000-0001-8520-8983>  
 Liliia Uvarova  <https://orcid.org/0000-0003-1448-0642>  
 Serhiy Rednyk  <https://orcid.org/0000-0002-0408-0170>  
 Štěpán Roučka  <https://orcid.org/0000-0002-2419-946X>  
 Erik Vanko  <https://orcid.org/0000-0001-6652-0066>  
 Petr Dohnal  <https://orcid.org/0000-0003-0341-0382>  
 Juraj Glosík  <https://orcid.org/0000-0002-2638-9435>

## References

- Atkins, P. W., De Paula, J., & Keeler, J. 2018, *Atkins' Physical Chemistry* (11th ed.; Oxford: Oxford Univ. Press)
- Cazzoli, G., & Puzzarini, C. 2006, *ApJL*, **648**, L79
- Chaizy, P., Réme, H., Sauvaud, J. A., et al. 1991, *Natur*, **349**, 393
- Cordiner, M. A., & Charnley, S. B. 2014, *MAPS*, **49**, 21
- Desai, R. T., Zhang, Z., Wu, X., & Lue, C. 2021, *PSJ*, **2**, 99
- Endres, C. P., Schlemmer, S., Schilke, P., Stutzki, J., & Müller, H. S. 2016, *JMoSp*, **327**, 95
- Endres, E. S., Egger, G., Lee, S., et al. 2017, *JMoSp*, **332**, 134
- Endres, E. S., Ndengué, S., Lakhmanskaya, O., et al. 2021, *PhRvA*, **103**, 052807
- Engelking, P. C. 1982, *PhRvA*, **26**, 740
- Gerlich, D. 1992, in *Advances in Chemical Physics: State-Selected and State-To-State Ion-Molecule Reaction Dynamics*, Part 1. Experiment, ed. C.-Y. Ng et al., Vol. 82 (New York: Wiley), 1
- Gerlich, D. 1995, *PhysS*, **T59**, 256
- Gerlich, D., Borodi, G., Luca, A., Mogo, C., & Smith, M. A. 2011, *ZPC*, **225**, 475
- Gerlich, D., Plašil, R., Zymak, I., et al. 2013, *JPCA*, **117**, 10068
- Glosík, J., Hlavenka, P., Plašil, R., et al. 2006, *RSPTA*, **364**, 2931
- Goldfarb, F., Drag, C., Chaibi, W., et al. 2005, *JChPh*, **122**, 014308
- Grabowski, J. J., DePuy, C. H., & Bierbaum, V. M. 1983, *JChS*, **105**, 2565
- Hauser, D., Lakhmanskaya, O., Lee, S., Roučka, Š., & Wester, R. 2015a, *NJPh*, **17**, 075013
- Hauser, D., Lee, S., Carelli, F., et al. 2015b, *NatPh*, **11**, 467
- Herbst, E. 1981, *Natur*, **289**, 656
- Hlavenka, P., Otto, R., Trippel, S., et al. 2009, *JChPh*, **130**, 061105
- Huber, K. P., & Herzberg, G. 1979, *Molecular Spectra and Molecular Structure*, Vol. IV, *Molecular Spectra and Molecular Structure: Constants of Diatomic Molecules* (New York: Van Nostrand Reinhold)
- Irikura, K. K. 2007, *JPCRD*, **36**, 389
- Jusko, P., Asvany, O., Wallerstein, A.-C., Brünken, S., & Schlemmer, S. 2014, *PhRvL*, **112**, 253005
- Jusko, P., Roučka, Š., Mulin, D., et al. 2015, *JChPh*, **142**, 014304
- Kolos, W., & Wolniewicz, L. 1967, *JChPh*, **46**, 1426
- Kovalenko, A., Roučka, Š., Tran, T. D., et al. 2021, *JChPh*, **154**, 094301
- Lee, S., Hauser, D., Lakhmanskaya, O., et al. 2016, *PhRvA*, **93**, 032513
- Light, J. C., Ross, J., & Shuler, K. E. 1969, in *Kinetic Processes in Gases and Plasmas*, ed. A. R. Hochtüm (New York: Academic), 281
- Matsushima, F., Yonezu, T., Okabe, T., Tomaru, K., & Moriwaki, Y. 2006, *JMoSp*, **235**, 261
- Mautner, M. M.-N., Lloyd, J. R., Hunter, E. P., Agosta, W. A., & Field, F. H. 1980, *JChS*, **102**, 4672
- McCarthy, M. C., Gottlieb, C. A., Gupta, H., & Thaddeus, P. 2006, *ApJL*, **652**, L141
- McElroy, D., Walsh, C., Markwick, A. J., et al. 2013, *A&A*, **550**, A36
- Meyer, C., Becker, A., Blaum, K., et al. 2017, *PhRvL*, **119**, 023202
- Millar, T. J., Walsh, C., & Field, T. A. 2017, *ChRv*, **117**, 1765
- Mukundan, V., & Bhardwaj, A. 2018, *ApJ*, **856**, 168
- Mulin, D., Roučka, Š., Jusko, P., et al. 2015, *PCCP*, **17**, 8732
- Nötzold, M., Wild, R., Lochmann, C., & Wester, R. 2022, *PhRvA*, **106**, 023111
- Otto, R., von Zastrow, A., Best, T., & Wester, R. 2013, *PCCP*, **15**, 612
- Plašil, R., Mehner, T., Dohnal, P., et al. 2011, *ApJ*, **737**, 60
- Plašil, R., Roučka, Š., Kovalenko, A., et al. 2022, *ApJ*, **941**, 144
- Plašil, R., Tran, T. D., Roučka, Š., et al. 2017, *PhRvA*, **96**, 062703
- Plašil, R., Zymak, I., Jusko, P., et al. 2012, *RSPTA*, **370**, 5066
- Roučka, Š., Rednyk, S., Kovalenko, A., et al. 2018, *A&A*, **615**, L6
- Rehfuss, B. D., Crofton, M. W., & Oka, T. 1986, *JChPh*, **85**, 1785
- Remijan, A., Scolati, H. N., Burkhardt, A. M., et al. 2023, *ApJL*, **944**, L45
- Rosenbaum, N. H., Owrutsky, J. C., Tack, L. M., & Saykally, R. J. 1986, *JChPh*, **84**, 5308

Schmidt, H. T., Eklund, G., Chartkunchand, K. C., et al. 2017, [PhRvL](#), **119**, 073001  
Schulz, P. A., Mead, R. D., Jones, P. L., & Lineberger, W. C. 1982, [JChPh](#), **77**, 1153  
Smit, A. L. C., & Field, F. H. 1977, [JChS](#), **99**, 6471  
Smith, J. R., Kim, J. B., & Lineberger, W. C. 1997, [PhRvA](#), **55**, 2036

Su, T., & Chesnavich, W. J. 1982, [JChPh](#), **76**, 5183  
Viggiano, A. A., & Morris, R. A. 1994, [JChPh](#), **100**, 2748  
Weinreb, S., Barrett, A. H., Meeks, M. L., & Henry, J. C. 1963, [Natur](#), **200**, 829  
Wyrowski, F., Menten, K. M., Güsten, R., & Belloche, A. 2010, [A&A](#), **518**, A26  
Zymak, I., Hejduk, M., Mulin, D., et al. 2013, [ApJ](#), **768**, 86